Enhancing the accuracy of the Leica Nova TS60 total station: A multi-purpose camera-based optical measurement system

Clemens Schuwerack[1], Lukas Quirin[1], Gunnar Lelle-Neumann[1], Ferdinand Maiwald[1]

[1] Chair of Optical 3D-Metrology, TU Dresden, 01069 Dresden, Germany –
(clemens.schuwerack, lukas.quirin, gunnar.lelle-neumann, ferdinand.maiwald)@tu-dresden.de

Keywords: 3D measurement system, image-assisted total station, QDaedalus, multi-purpose, deformation analysis, high accuracy.

Abstract

The increasing demand for accurate 3D coordinate measures in industry, medicine and environmental sciences often comes with multiple constraints regarding the object distance, required accuracy and object signalization. While many systems are specialized in one domain, there are only few systems that operate in close-range applications with extremely high accuracy and are also capable of monitoring deformations at a distance of a few hundred meters. Therefore, a measurement system based on the astro-geodetic observation system QDaedalus is introduced using two combined image-assisted total stations (IATS) Leica NOVA TS60. By combining exact collimation, camera calibration and spatial intersection we show in several close-range experiments that our system is capable of measuring various kind of targets with a 3D point accuracy below 0.01 mm.

1. Introduction

Advancements in technology have driven an increasing need for precise 3D measurement systems across diverse fields, including manufacturing, medical imaging, and environmental monitoring. These applications often require systems that can meet specific constraints, such as capturing measurements at variable distances, achieving high levels of accuracy, and accommodating specific methods of target identification or signalization. Most existing 3D measurement systems are tailored for single-use scenarios or specific domains, limiting their versatility. Only a few systems are capable of achieving both ultra-precise measurements in close-range scenarios and accurate tracking of deformations over larger distances. Such systems are especially valuable in applications where flexibility in measurement distance and high accuracy are critical for reliable data acquisition and monitoring over time.

Therefore, we further developed a system which uses two synchronized total stations equipped with CCD cameras at the position of the eye-piece (Fig. 1), formerly introduced by researchers of the ETH Zurich as QDaedalus for astro-geodetic observations (Burki et al., 2010; Guillaume et al., 2012). Firstly, the system utilizes the high accuracy of the internal angle encoders in the total station which improves the angular accuracy by factor 3. Secondly, we perform a principal point calibration for the external camera and evaluate the images using sub-pixel algorithms. The use and control of CCD cameras and algorithms in our Python-based interface also enables automated measurements.

In our experiments, we were able to measure the close-range 3D position of different types of targets (elliptical, cross-shaped, illuminated) during multiple experiments with an accuracy of < 0.01 mm. While this accuracy is within the range of modern laser tracker systems, our system has the advantage of being less expensive and able to measure different types of targets using image analysis. This allows flexible optical industrial measurements without any tactile influence. Points can be signalized using conventional markers, but we show that also natural points can be detected and measured in multiple sets.

Figure 1. Setup of the two total stations TS60-1 (A), TS60-2 (B) and the observed objects in the geodetic measurement lab at TU Dresden. The origin of the right-handed coordinate system lies in TS60-1 and the x-axis points towards TS60-2 after the base line determination using exact collimation.

2. Related Work

First systems that introduce cameras to electronic tacheometers were developed at the ETH Zurich (Matthias, 1991) based on the original approaches introduced in e.g., Gottwald (1987) and Huep (1988). By integrating external eye-piece cameras to tacheometers, it was possible to accurately measure zenith angles between 170 and 230 gon which initially allowed the use for applications in pithing (Knoblach, 2009) and for astro-geodetic observations (Burki et al., 2010). Specifically, this astro-geodetic system DAEDALUS by the ETH Zurich (Burki et al., 2010) was later further improved by an extended research group for terrestrial close-range measurements using the properties of the tacheometers angle encoders and image analysis procedures (Guillaume et al., 2012). Charalampous et al. (2014) included the Guppy-F-080C CCD camera as external eye-piece which allowed external triggering with a frame rate

of 60 frames per second (fps). Further, they implemented image analysis methods for Optical Target Recognition (OTR) such as the determination of the center of mass, template least squares matching, and circle matching (Guillaume et al., 2012). This allowed monitoring of a rigid structure with two QDaedalus theodolites in a distance of $5 - 6$ m with standard deviations in the direction of vertical displacements lower than 0.03 mm. Guillaume et al. (2016) were able to adapt the system to a Leica MS50 total station reaching a standard deviation for 3D coordinates with approximately 0.01 mm. Regarding the initial purpose of the DAEDALUS system, also the QDaedalus system was later used for astro-geodetic observations (Hauk et al., 2016; Völgyesi and Tóth, 2021; Albayrak et al., 2022).
For close-range to mid-range displacement measurements more recently Paar et al. (2021) mounted a GoPro on a Leica TPS1201 and dynamically measured bridge deformations on mm-level while the MoDiTa system by Zschiesche et al. (2022) uses self-calibrated industrial cameras mounted on a Leica MS50 total station and resolves micro-movements of 0.5 mm / 100 m. Further, there exist several comprehensive reviews on the topic of image-assisted total stations (IATS) (Ehrhart and Lienhart, 2015; Zschiesche, 2021). Our depicted system differs from the above-mentioned methods by using a combination of two collimated IATS with different industrial cameras initially in a close-range setting, while also maintaining a point accuracy of < 0.01 mm.

3. Experimental Setup

This section is divided into two parts. Firstly, we will introduce the hardware and software used for our modification of the QDaedalus system and explain the process of collimation and coordinate estimation. Secondly, the three different experiments and their evaluation are described.

3.1 Hardware

This section describes the properties of the total stations, the external cameras and the different targets that were used for the experiments.

3.1.1 Theodolite Measurement System Conventional industrial theodolite measurement systems combine the angular measurements from a minimum of two theodolites/total stations for the calculation of 3D point coordinates using spatial intersection. These systems formerly achieved a 3D point coordinate accuracy of $\sigma_{XYZ} = 2 - 8$ mm (Zhang et al., 2012) up to $\sigma_{XYZ} = 0.03$ mm (Charalampous et al., 2014). For our experiments we used the angular measurement function of two total stations Leica NOVA TS60. The TS60 features not only the conventional functions of a tachymeter, such as distance, horizontal direction, and vertical angle measurements, but also advanced functionalities such as a laser scanning unit and a camera unit. For the purposes of our experiments, the primary focus will be on horizontal and vertical angle measurements using the values derived directly from the internal angle encoders. According to the datasheet, the TS60 offers an angular measurement accuracy of $\sigma_{TS60} = 0.15 mgon$. However, direct angle encoder accuracy is given for comparable devices as $\sigma_{Hz} = 0.018$ mgon for the horizontal angle and $\sigma_V = 0.028$ mgon for the vertical angle (Zogg et al., 2009) which could lead to a theoretical 3D point accuracy of $\sigma_{XYZ} = 0.004$ mm in a distance of 10 m for a single system.

3.1.2 Camera System For our experiments we did not use the original camera system as described in Knoblach (2009) and Burki et al. (2010). The external camera used is the Guppy Pro F-031 B by AVT with an image resolution of 656 x 492 pixels. This camera is mounted on the eyepiece of the total stations and transmits the optics of the telescope. The Guppy PRO F-031B model is a monochrome camera equipped with a Sony ICX618 CCD sensor. A FireWire interface powers the camera and enables image data transmission via a 800 Mb/s connection. When mounted on the TS60, the camera operates without a lens. It features a standardized C-Mount thread connection (Schuwerack, 2021). The selection of the camera for the experiments is based on decisions by Burki et al. (2010) and has the main advantage of enhancing the original angle measurement accuracy from $0.5''$ (0.15 mgon) to approximately $0,2''$ (0.05 mgon) by using camera calibration and moment/ellipse detection.

Furthermore, continuous image streaming enables to use the system for real-time observation (Guillaume et al., 2016). With the attached Guppy camera the image plane does not coincide with the CCD sensor plane anymore and objects at a certain range move out of focus. This can be circumvented by installing a meniscus lens in front of the objective lens (Guillaume et al., 2012).

3.1.3 Targets For the experiments in section 3.5, different types of targets were used (Fig. 2). The AICON target markers consist of a center and a cyclic binary code that surrounds this center. These targets enable the determination of the marker's center, using OTR such as an ellipse or center of gravity operator algorithm regardless of the positioning and rotation. The cyclic code is used to assign a fixed ID to the resulting point (coded target). The circle target markers work by the same principle, the only difference is the absence of the cyclic code. For these markers and their resulting points the IDs have to be assigned manually (uncoded target).
In addition, two LED target markers where used. One of them is a conventional LED, placed on a dark foam pad. The other LED target is covered in an opaque transparent sphere that emits a more uniform light. This spherical LED was used for calibrating the cameras of the theodolite measurement system. In section 3.5.1 various target markers and detection algorithms were tested with regard to their influence on the accuracy of the point coordinate measurements.

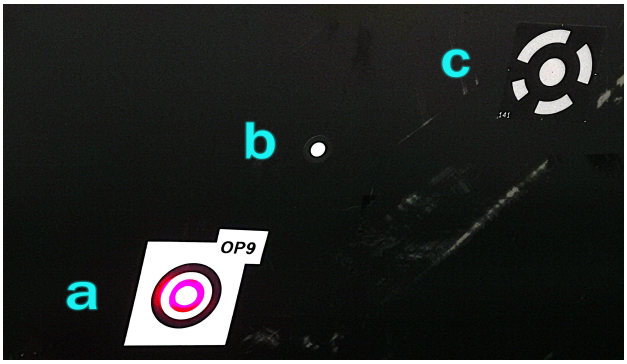

Figure 2. Circle target markers (a and b) and AICON target marker (c) used for the experiments.

3.2 Software

Full remote access to the motorization, measuring instruments and camera of both total stations and for implementing automa-

tion is realized by the company's internal serial communication interface GeoCOM (using RS232). The remote control enables the non-tactile vertical and horizontal movement of the total station and especially the change to the second telescope position (Face II). This system is based on a Remote Procedure Call (RPC), which communicates in ASCII2 format. This format allows to send requests to the total station for retrieving instrument data, instrument control and error handling (Leica Nova MS50: GeoCOM Reference Manual, 2024). Wireless interface alternatives are Bluetooth or WiFi (Leica Nova MS60: Datenblatt, 2020). The different components are connected through a computer unit with compatible interfaces. In order to design the implementation independently from the OS, a Graphical User Interface (GUI) was designed based on the *PyQt5* library and *QtDesigner* (Fig. 3). Therefore, we complemented the existing repository `https://github.com/siyka-au/pygeocom` with additional GeoCOM commands. The GUI enables interactions, such as clicking on a position in the camera stream to be approached. In the camera stream, the current principal point is permanently displayed in the form of a red crosshair, which reflects the aiming of the total station in the image space. Also the calibration process is controlled via the GUI. Further actions allow controlling the focus lens position, direct control of horizontal and vertical angle, changing camera parameters such as gain and exposure time, and the OTR.

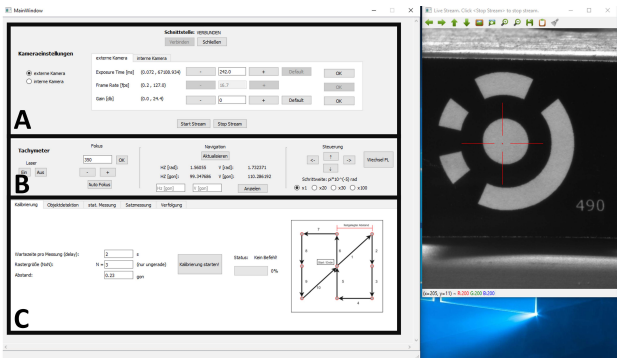

Figure 3. The GUI of the optical measurement system which allows manipulation of the camera parameters (A), control of the total stations (B), and instructions for calibration (C). On the right-hand side the live-view of the cameras can be visualized (Schuwerack, 2021)

3.3 Optical Target Recognition

For automatic detection of targets, the system is only roughly guided into the direction of the specific marker. Several image analysis methods for OTR and determination of the target's center are implemented in the software used and can be directly applied in the camera stream. These include moment detection, line detection using Hough transform, contour detection, circle and ellipse detection. In prior experiments it was shown that especially the moment detection (Hu, 1962) is suitable for highly accurate LED detection while ellipse detection (Kanatani et al., 2016) is more suitable for determining the center coordinates of the flat black and white circular markers Schuwerack (2021). This is why we choose these methods for the experiments in section 3.5.

3.4 Measurement Workflow

Reaching the high accuracies requires using the following procedure including camera calibration, base length estimation and spatial intersection. As a first step, principal point calibration is performed to define the center of the telescope´s optical axis with the CCD chip of the camera. As a next step, the baseline between both instruments needs to be determined to define the local coordinate system. After that, 3D point coordinates can be determined using spatial intersection which leads to the performed experiments.

3.4.1 Principal Point Calibration Process In the measurement system the principal point is defined as the intersection of the telescope's optical axis with the plane of the CCD chip. According to Knoblach (2009) the transformation between sensor plane of the camera and spherical angular space of the total station can be realized via affine transformation. Therefore, a target grid in object space pointing at different places on the CCD chip is observed multiple times (Fig. 4). This allows the estimation of the principal point with a precision of $< 1/10$ pixel in a bundle adjustment procedure (Schuwerack, 2021).

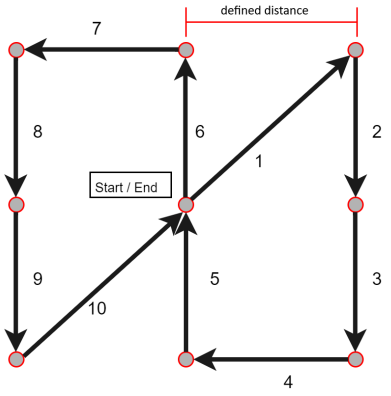

Figure 4. Schematic diagram of the calibration routine (Schuwerack, 2021).

3.4.2 Coordinate System Definition and Base Line Determination The idea for orientation and point measurement of the system can be compared to photogrammetric principles spatial resection and intersection. As our system uses two total stations, both systems need to be precisely relatively aligned in order to measure similar object coordinates. This is realized by reciprocal targeting of both instruments in two telescope positions also known as exact collimation. Therefore, the laser plummet of instrument B is mirrored into the direction of instrument A and vice versa, while instrument A serves as origin with coordinates $A(0, 0, 0)$ (Fig. 5).

The center of the projected laser dot is determined using the implemented centroid (moment) estimation (see 3.3). This defines the direction of the x-axis (Fig. 1 and Fig. 6) and the location of instrument B at $B(d_{AB} = b, 0, \Delta h_{AB})$, where Δh_{AB} represent the height difference between the two total stations.

As the length of the base b between the instruments is initially not measurable within the high accuracy requirement, it is approximated as $b_0 = 1$ and estimated in an iterative process. Therefore, a subtense bar is placed within the scene for which the reference length L was determined a priori through multiple interferometric measurements with a standard deviation $\sigma_L = 1.4$ µm.

Then, both endpoints $P_1(X, Y, Z)$ and $P_2(X, Y, Z)$ of the bar are again determined with measurements of the described sys-

Figure 5. Exact collimation with the two total stations Leica NOVA TS60-1 and TS60-2. The mirrored laser plummet target is visible underneath each total station.

tem using triangulation. Point coordinates are calculated using Equations 1 to 3.

$$X_P = b \cdot \frac{\sin(\beta) \cdot \sin(\alpha)}{\sin(\alpha + \beta)} \tag{1}$$

$$Y_P = b \cdot \frac{\sin(\beta) \cdot \cos(\alpha)}{\sin(\alpha + \beta)} \tag{2}$$

$$Z_P = \frac{1}{2} b \cdot \frac{\sin(\beta) \cdot \cot(\zeta_A) + \sin(\alpha) \cdot \cot(\zeta_B)}{\sin(\alpha + \beta)} + \Delta h_{AB} \tag{3}$$

As for the calculation of Z_P, the zenith angle of the total stations is also used to estimate Δh_{AB} as shown in Equation 4:

$$\Delta h_{AB} = \frac{1}{2} b \cdot \left(\frac{\sin \alpha_1 \cot \zeta_{B1} - \sin \beta_1 \cot \zeta_{A1}}{\sin(\alpha_1 + \beta_1)} + \frac{\sin \alpha_2 \cot \zeta_{B2} - \sin \beta_2 \cot \zeta_{A2}}{\sin(\alpha_2 + \beta_2)} \right) \tag{4}$$

and finally the estimation of the subtense bar length L_0 is calculated by these approximated point coordinates using euclidean distance (Eq. 5)

$$L_0 = \sqrt{(X_1 - X_2)^2 + (Y_1 - Y_2)^2 + (Z_1 - Z_2)^2} \tag{5}$$

Base length b is now determined in an iterative process with

$$b = b_0 \frac{L}{L_0}, \tag{6}$$

where the approximated bar length L_0 is converging to the interferometric length L. The process is stopped when the convergence criteria reaches

$$|L - L_0| \leq 0.01\ mm. \tag{7}$$

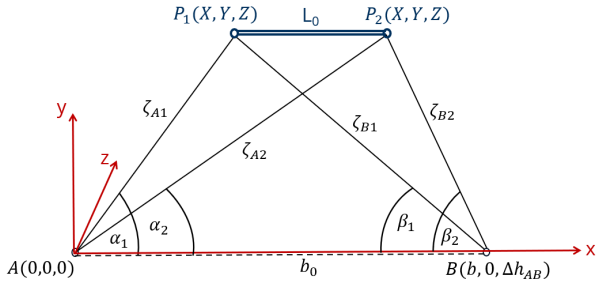

Figure 6. Schematic representation of the base length determination using collimation and iterative spatial intersection.

3.4.3 Determination of 3D coordinates With the calibrated camera and the fixed base line, coordinates of target points can be directly determined in the local total station coordinate system using exclusively the angle measurements and spatial intersection in object space. Using measurements of at least three object points allows for the transformation into an arbitrary object coordinate system using e.g. a 7-parameter-transform or 3-2-1 Euler angles. Due to the implemented image analysis methods, it becomes possible to measure multiple kinds of targets, e.g., illuminated targets, geodetic targets, and photogrammetric targets. Once detected, the targets can be repetitively measured in two faces by saving the initial position and finding the new position of the target in the images in the next epoch. The time between epochs can be freely selected, theoretically allowing long-time monitoring in environmental applications, or high-frequency analysis of short-time movements e.g., in industrial applications.

3.5 Experiments

To achieve optimal accuracy in angular measurements, we initially identified the most effective targets in experiment 1. The approved and selected targets were then used for experiments 2 and 3. In experiment 2 we undertook measurements to assess only few coordinates of target points on a structure allowing a rough estimate of the expected accuracy of our system. In experiment 3 the amount and distribution of target points was significantly increased. The results are then shown in section 5.

3.5.1 Experiment 1: Accuracy of Different Target Types In this experiment, we determined the horizontal and vertical angle measurement accuracy for different targets. The basic measurement setup is shown in Figure 1. The two total stations introduced in section 3.1.1 were used for simultaneous measurements in accordance to DIN ISO 17123-3 (2001). The five target positions were distributed around the horizon by approx. 200 gon (Fig. 7). For the limited space available in the lab, an arrangement around the entire horizon was not possible. The

targets were positioned at distances of approx. 3m to 6m from the total station TS 60-2. The distances to the TS 60-1 range from 3m to 9m. The targets were aligned facing TS 60-2. For reasons of clarity, Figure 7 shows the directions of observation only for one instrument (TS 60-2). For the TS 60-1, the measurements for targets 2, 3 and 4 were carried out on obliquely aligned target panels. This approach seeks to examine the potential influence of skewed targets on the measurement. In this context, *skewed* refers to those that are not perfectly facing into the direction of the instrument. The test field was configured to optimally meet the requirements for assessing the accuracy of horizontal alignment measurements in our laboratory. Measurements with a modified measurement setup for the vertical angle, as described in DIN ISO 17123-3 (2001), were not carried out. The coverage of the vertical circle is only about 10 gon. A target plate was prepared for each target direction with the different targets markers to be examined. The measuring system was calibrated before each series of measurements. We tested all four different target marker types described in section 3.1.3.

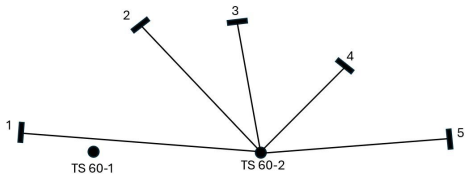

Figure 7. Experimental setup with the total stations TS60-1, TS60-2 and the measurement positions 1-5.

Further, the centers of the LED targets were detected by moment detection while the AICON and circle target were determined using ellipse detection in the developed software as done in earlier experiments (Schuwerack, 2021).

3.5.2 Experiment 2: Small Amount of Targets DIN ISO 17123-3 (2001) specifies a field method for determining and assessing the repeatability of theodolite measurements, in this case, the TS60 total stations. The measurement setup and the measurement procedure are based on these specifications. However, the execution of the experiments did not strictly follow the test procedure in DIN ISO 17123-3 (2001). The objective is to evaluate the measurement accuracy of the developed measurement system with regard to the algorithms used, the two camera systems and two target types. Furthermore, this assessment aims to assess whether the accuracy of the image measurement achieved is superior to that of a conventional total station measurement. The total station is mounted on a steel pillar anchored in the wall of the laboratory to provide the required stability. The five measurement points are attached on a car door model in a vertical column (Fig. 8 (d)). The car door is slightly arched, so that the points also differ in x- and y-direction.

After calibration and exact collimation, the measurements are carried out as classic set measurements. In each case, five measuring points were measured in four sets, each set includes the measurements from both the first and second telescope positions (Face I / Face II) for each target point. The four measurement sets were conducted automatically. After training the total stations in one training set, each learned point was targeted automatically by the total stations. The training was conducted according to the following procedure for each total station: First, we manually aimed at the point to be measured (target marker) with the target laser of the total station. Focusing was

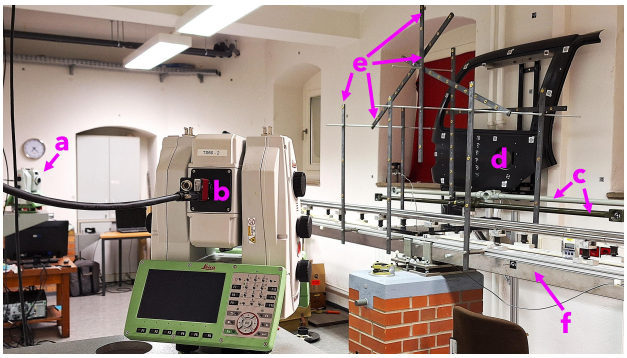

Figure 8. Experimental setup with TS60-1 (a) and TS60-2 (b) (each equipped with a Guppy camera), subtense bars (c) for the base line determination, car door for experiment 2 (d), additional structure for experiment 3 (e) and the mounting rail (f).

carried out via the GUI. Then we defined a region of interest (ROI) around the target in the image stream output of the GUI. Next, we targeted the center of the target marker in the image stream with a mouse click. The outline of the target marker is then determined using an ellipse detection algorithm. The algorithm calculates the center of the ellipse. When the pixel accuracy shown in the live stream is sufficient and stable, the position is saved and the direction measurement can be started. The same procedure can now be followed for the next measuring point.

3.5.3 Experiment 3: Large Amount of Targets Experiment 2 showed promising results (sec. 4.2). So, in order to increase the variety of x-, y- and z-coordinates and the variety of distances to the total stations, an additional three dimensional bar structure was mounted on the rail system of the laboratory. The structure can be seen in Figure 8 (e). Experiment 3 was conducted in the same way as experiment 2. The measurements were repeated on two consecutive days. The measurement procedure was the same on both days, also the calibration was carried out again. In comparison with experiment 2, we increased the amount of target points to a total number of 30 points. These 30 points were measured in twelve sets of which eight were used for the evaluation on each day (sec. 4.3).

4. Results

In this section the results for the accuracy assessment for the target marker type (experiment 1) and the target point measurement (experiment 2 and 3) are presented.

4.1 Experiment 1: Different Targets

The results of the target marker tests are shown in Table 1. The empirical standard deviations were calculated in accordance with DIN ISO 17123-3 (2001) from four measurement series from different measurement days. In principle, two measurement series from day (A) and one measurement series each from day (B) and (C) were used for each target character. Accordingly, the camera was recalibrated before each series of measurements and the target characters were retrained.

With the two adhesive markers, the highest accuracies were achieved. No significant impact on the attainable directional and angular measurement accuracy was observed, even when measurements were conducted on target plates that were not optimally aligned or under irregular lighting conditions. As

	TS 60-1	
	s_{Hz} (mgon)	s_V (mgon)
circle	0.047	0.041
AICON	0.045	0.036
spherical LED	0.055	0.045
conv. LED	0.054	0.064
	TS 60-2	
	s_{Hz} (mgon)	s_V (mgon)
circle	0.043	0.038
AICON	0.044	0.044
spherical LED	0.054	0.058
conv. LED	0.068	0.069

Table 1. Achieved accuracies for the different target markers

shown in Table 1 the empirical standard deviations s_{Hz} for both LEDs are distinctly larger than with the two adhesive markers. Depending on the size and distance of the target, we decided to use the smaller simple dot marker and the larger retro-reflective "AICON" marker for the experiments 2 and 3. For the camera calibration, we used the spherical LED target. For the flat targets a consistent empirical standard deviation of $< s_{Hz} = 0.05$ mgon is reached.

4.2 Experiment 2: Small Amount of Targets

Table 2 shows the standard deviations for the results of experiment 2, which are a measure of the 3D point accuracy achieved in the measurements. The points with IDs 141, 142 and 143 are used for the definition of the object coordinate system. The actual measurement targets are the object points with IDs 36 - 40, using flat AICON markers. The aim for our experiments was to show that the system reaches a 3D point accuracy of $\sigma_{XYZ} < 10$ µm. For each coordinate value X, Y, Z the mean standard deviation $\overline{s}_i = \frac{\sum(s_i)}{n}$ with $n = 5$ was calculated. The overall accuracy was determined with $\sigma_{xyz} = \sqrt{\overline{s}_x^2 + \overline{s}_y^2 + \overline{s}_z^2}$. As shown in Table 2, we could achieve a final accuracy of $\sigma_{xyz} = 4.0$ µm.

ID	s_x (µm)	s_y (µm)	s_z (µm)
141	0.0	0.0	0.0
142	1.5	0.0	1.9
143	0.7	0.0	0.0
36	3.0	1.4	1.9
37	2.5	3.4	1.7
38	2.1	3.6	2.1
39	2.9	1.3	1.5
40	1.5	3.3	1.8
	$\overline{s}_x$ (µm)	$\overline{s}_y$ (µm)	$\overline{s}_z$ (µm)
	2.4	2.6	1.8
σ_{xyz} (µm)	**4.0**		

Table 2. Standard deviations of the x-, y- and z-values and accuracy derived from the direction measurements in experiment 2.

4.3 Experiment 3: Large Amount of Targets

The results of experiment 3 confirm the achieved accuracies in experiment 2. The standard deviations of the measurements of both days are shown in Table 3. The calculation of the standard deviation was carried out for each day with eight out of twelve sets. For each coordinate direction for day 1 and day 2 respectively, the mean standard deviation $\overline{s}_i = \frac{\sum(s_i)}{n}$ with $n = 30$ was calculated. The accuracy was determined with $\sigma_{xyz} = \sqrt{\overline{s}_x^2 + \overline{s}_y^2 + \overline{s}_z^2}$. In our experiments, we could reach accuracies of $\sigma_{xyz} < 10$ µm (Tab 3). Deviations are within the

	exp.3 - day 1			exp. 3 - day 2		
ID	s_x (µm)	s_y (µm)	s_z (µm)	s_x (µm)	s_y (µm)	s_z (µm)
COL	4.3	2.2	4.5	5.8	5.6	7.6
BL	0.9	2.4	1.7	1.8	3.5	3.3
BR	0.9	4.2	1.5	1.8	1.2	4.1
101	0.0	0.0	0.0	0.0	0.0	0.0
34	2.0	0.0	1.9	3.3	0.0	6.7
71	4.0	0.0	0.0	3.1	0.0	0.0
81	***6.3***	5.7	3.3	3.2	2.1	1.4
84	3.0	4.2	1.3	2.5	2.3	2.0
102	1.9	3.1	1.1	1.5	2.6	1.1
104	1.8	2.0	1.4	1.1	1.5	1.7
41	3.7	2.9	2.0	3.0	3.7	2.2
44	3.0	2.7	1.6	4.6	3.0	1.9
91	2.9	2.9	0.9	6.5	***6.8***	5.2
94	3.6	3.3	1.3	2.5	4.1	2.8
31	1.6	2.2	1.4	2.3	1.2	1.3
33	2.7	1.8	1.7	2.2	3.7	1.9
61	5.8	2.7	1.7	5.1	2.8	2.8
64	5.4	2.9	2.0	5.7	3.7	3.0
72	3.0	2.0	1.8	3.9	2.0	1.3
74	3.1	1.5	1.5	4.3	4.4	1.9
11	1.7	2.2	1.2	2.6	3.1	1.4
14	3.7	2.4	2.2	3.6	3.7	***1.0***
21	3.7	2.9	1.4	3.6	2.5	1.7
24	2.5	2.2	1.4	2.4	3.8	1.4
51	2.0	2.7	1.8	2.9	2.8	2.0
54	1.1	2.6	1.4	2.7	2.8	2.6
111	2.2	1.7	1.7	3.2	3.1	2.4
114	1.6	3.1	1.1	2.9	4.5	1.8
121	1.9	1.3	1.4	2.4	1.5	1.6
124	1.9	1.1	1.8	2.6	3.4	2.1
142	1.8	2.0	0.9	2.6	2.0	1.8
136	2.5	1.7	1.0	2.5	3.0	2.4
137	1.4	2.7	***0.8***	3.2	2.6	1.5
138	2.4	3.2	1.2	2.8	2.7	2.1
139	2.5	2.0	1.7	3.0	2.2	1.9
140	3.3	3.3	2.0	2.5	1.6	1.5
	$\overline{s}_x$ (µm)	$\overline{s}_y$ (µm)	$\overline{s}_z$ (µm)	$\overline{s}_x$ (µm)	$\overline{s}_y$ (µm)	$\overline{s}_z$ (µm)
	2.8	2.6	1.5	3.1	3.0	2.0
σ_{xyz} (µm)	**4.1**			**4.8**		

Table 3. Standard deviations of the x-, y- and z-values derived from the direction measurements in experiment 3. Calculated accuracies σ_{xyz} below. Targets with IDs 136 - 140 and 142 had AICON markers.

expected range. For each measurement day, the minimum and maximum standard deviation is highlighted in the table. The records of sets 1, 2, 7 and 11 for day 1 and the records of sets 2, 5, 11 and 12 for day 2 were not considered for further analysis and removed as outliers, because their means of standard deviations were greater than $\overline{s}_i > 10$ µm.

The points with IDs COL, BL and BR were used in the calibration process for the collimation and for the end points ("bar left" and "bar right") of the base bar L_0. The base bar length was controlled with sufficient accuracy ($\sigma_{XYZ} < 0.05$ mm). Point 101 is our coordinate system origin, while the points 34 and 71 define the axis directions. All three points are located on the bar structure. The remaining 30 points were considered for the evaluation. The points 111, 114, 121, 124, 136 - 140 and 142 located on the car door model, all other measurement points were located on the structure. For the six points 136 - 140 and 142 we used AICON markers, for all other points we used the simple circle markers.

Comparing the mean coordinate values of the eight sets of day 1

ID	dx (µm)	dy (µm)	dz (µm)
COL	-19.1	-0.9	4.4
BL	1.4	5.3	17.4
BR	0.5	7.9	-19.7
101	0.0	0.0	0.0
34	6.6	0.0	1.1
71	-1.2	0.0	0.0
81	-10.7	2.6	1.4
84	5.1	2.6	-0.1
102	-2.8	4.0	2.5
104	-8.0	-1.4	1.9
41	0.1	7.8	6.9
44	12.4	6.7	4.8
91	4.9	4.6	0.2
94	1.4	7.5	2.5
31	1.4	4.9	0.5
33	0.7	5.9	-0.1
61	3.0	8.2	-0.9
64	6.5	-0.5	-0.9
72	3.1	0.8	1.9
74	4.0	1.2	2.4
11	4.4	6.3	-0.4
14	0.7	8.8	0.4
21	5.7	0.1	1.1
24	6.1	12.1	4.5
51	3.1	2.4	-8.8
54	4.7	7.1	9.9
111	**-25.0**	4.2	-0.7
114	**-23.8**	8.0	-1.6
121	**-29.8**	0.5	-0.6
124	**-26.6**	5.6	-0.9
142	**-23.9**	3.8	-0.4
136	**-30.0**	3.4	-1.1
137	**-25.7**	4.4	-0.9
138	**-26.7**	2.0	0.1
139	**-26.5**	0.2	1.1
140	***-44.2***	***22.2***	***31.2***

Table 4. Subtracting coordinate values of day 1 from the values of day 2 gives the differences di for each direction.

with the mean coordinates of the eight sets of day 2 (Tab. 4), the coordinates reveal a remarkable shift in x-direction. The shift only occurs for certain points: The only points affected by the shift are located on the car door, which indicates a relative movement between the car door and the bar structure over night. The most likely explanation is a temperature change in the laboratory, causing the rail system to expand or to shrink. Since the origin point is located on the bar structure, which in turn is mounted on the rail system, the points on the car door show the shift. The differences in the measurement values for point 140 indicate a general outlier. The temperature aspect was not a planned or expected part in the experiments, but show quite well, that also structural changes in the range of $20 - 50$ µm are traceable with the developed system.

5. Conclusions and Outlook

We demonstrated the combined use of two IATS for our close-range industrial theodolite measurement system increasing the 3D point accuracy to < 0.01 mm while also being less expensive than conventional lasertracker systems. This is possible due to the introduction of principal point calibration of the externally mounted camera, exact collimation between the IATS and advanced target detection. We have shown that it is possible to detect various targets with our system while maintaining the demonstrated accuracy. Further, it has been shown that small deformations can be effectively detected by using measurements of different epochs and that the system accuracy stays stable between longer measurement periods. Still, there is potential for improvements.

The orientation and coordinate definition of the depicted system is at the moment based on exact collimation using the built-in laser plummets and their detection using moment estimation. However, we believe that this might introduce small errors which could be omitted in the future by using an initial approximate collimation and subsequent bundle adjustment. Further, the system is operated using two separately controlled total stations with two PCs. In the future, we intend to integrate a minimum of two total stations within our software on one single PC with additional online assessment and exchange of measured values. Regarding the possibility of extracting the full camera streams with 60 to 120 Hz, we made initial tests on time synchronization by using GNSS signals which would allow online deformation analysis or vibration measurements of targets. Additionally, a further improvement and more efficient use of the detection algorithms could eventually be used to automatically aim any type of structure, not only the ellipsoids or target markers respectively. First experiments have been carried out using the system in a natural environment observing larger volumes in distances up to 100 m which could be useful for measurement of sizable marine vessels or those that are challenging to access physically, like volcano surveillance or monitoring bridges at risk of collapse.

6. Acknowledgements

We want to thank Leander Brockes who performed a part of the experiments in section 3.5.1 observing different targets as a part of his thesis.

References

Albayrak, M., Willi, D., Guillaume, S., 2022. Field comparison of the total station-based QDaedalus and the zenith telescope-based CODIAC astrogeodetic systems for measurements of the deflection of the vertical. *Survey Review*, 55(390), 247–259.

Burki, B., Guillaume, S., Sorber, P., Oesch, H.-P., 2010. Daedalus: A versatile usable digital clip-on measuring system for total stations. *2010 International Conference on Indoor Positioning and Indoor Navigation*, IEEE.

Charalampous, E., Psimoulis, P., Guillaume, S., Spiridonakos, M., Klis, R., Bürki, B., Rothacher, M., Chatzi, E., Luchsinger, R., Feltrin, G., 2014. Measuring sub-mm structural displacements using QDaedalus: a digital clip-on measuring system developed for total stations. *Applied Geomatics*, 7(2), 91–101.

DIN ISO 17123-3, 2001. Optik und optische instrumente - feldprüfverfahren geodätischer instrumente - teil 3: Theodolite. Technical report, NA 005-03-04 AA.

Ehrhart, M., Lienhart, W., 2015. Monitoring of Civil Engineering Structures using a State-of-the-art Image Assisted Total Station. *Journal of Applied Geodesy*, 9(3).

Gottwald, R., 1987. Kern E2-SE - Ein neues Instrument nicht nur für die Industrievermessung? *Allgemeine Vermessungs-Nachrichten 4*.

Guillaume, S., Bürki, B., Griffet, S., Durand, H. M., 2012. Qdaedalus: Augmentation of total stations by ccd sensor for automated contactless high-precision metrology. *FIG Working Week 2012*.

Guillaume, S., Clerc, J., Leyder, C., Ray, J., Kistler, M., 2016. Contribution of the image-assisted theodolite system qdaedalus to geodetic static and dynamic deformation monitoring. *3rd Joint International Symposium on Deformation Monitoring (JISDM)*.

Hauk, M., Hirt, C., Ackermann, C., 2016. Experiences with the QDaedalus system for astrogeodetic determination of deflections of the vertical. *Survey Review*, 49(355), 294–301.

Hu, M.-K., 1962. Visual pattern recognition by moment invariants. *IEEE Transactions on Information Theory*, 8(2), 179–187.

Huep, W., 1988. Konzeption und einsatzmöglichkeiten eines automatisierten theodolitsystems. *X. Internationaler Kurs für Ingenieurvermessung*.

Kanatani, K., Sugaya, Y., Kanazawa, Y., 2016. *Ellipse Fitting for Computer Vision: Implementation and Applications*. Springer International Publishing.

Knoblach, S., 2009. Entwicklung, Kalibrierung und Erprobung eines kameraunterstützten Hängetachymeters. PhD thesis, TU Dresden.

Leica Nova MS50: GeoCOM Reference Manual, 2024.

Leica Nova MS60: Datenblatt, 2020.

Matthias, H., 1991. Der Robotertheodolit TOPOMAT - Technik, Anwendung und Auswirkung auf den Beruf. *Vermessung, Photogrammetrie, Kulturtechnik*.

Paar, R., Roić, M., Marendić, A., Miletić, S., 2021. Technological Development and Application of Photo and Video Theodolites. *Applied Sciences*, 11(9), 3893.

Schuwerack, C., 2021. Automatische zielverfolgung unter verwendung der intern verbauten kameras einer leica nova ts60. Master's thesis, TU Dresden.

Völgyesi, L., Tóth, G., 2021. Improvement of QDaedalus measurements with continuous detection of environmental parameters. *Acta Geodaetica et Geophysica*, 56(4), 607–622.

Zhang, X., Zhu, Z., Yuan, Y., Li, L., Sun, X., Yu, Q., Ou, J., 2012. A universal and flexible theodolite-camera system for making accurate measurements over large volumes. *Optics and Lasers in Engineering*, 50(11), 1611–1620.

Zogg, H.-M., Lienhart, W., Nindl, D., 2009. Leica ts30: The art of achieving highest accuracy and performance. Technical report, Leica Geosystems AG.

Zschiesche, K., 2021. Image Assisted Total Stations for Structural Health Monitoring—A Review. *Geomatics*, 2(1), 1–16.

Zschiesche, K., Fitzke, M., Schlüter, M., 2022. Self-Calibration and Crosshair Tracking with Modular Digital Imaging Total Station. *PFG – Journal of Photogrammetry, Remote Sensing and Geoinformation Science*, 90(6), 543–557.